



Anomalous relative intensity noise transfer in ultralong random fiber lasers

SERGIO ROTA-RODRIGO,^{1,*}  GIUSEPPE RIZZELLI,^{2,3} DANIEL LEANDRO,⁴  J. NUÑO,⁵ MANUEL LOPEZ-AMO,⁴  GIORGIO SANTARELLI,¹  AND JUAN DIEGO ANIA-CASTAÑÓN²

¹LP2N, IOGS, CNRS, Université de Bordeaux, 33400 Talence, France

²Instituto de Óptica “Daza de Valdés”, CSIC, Madrid, Spain

³Politecnico di Torino, Department of Electronics and Telecommunications (DET), Torino, Italy

⁴Universidad Pública de Navarra (UPNA) and Institute of Smart Cities (ISC), Navarra, Spain

⁵Universidad de Alcalá de Henares (UAH), Madrid, Spain

*sergio.rota2@gmail.com

Abstract: We present, for the first time, an experimental demonstration of RIN noise transfer dampening at low frequencies in random distributed feedback ultralong Raman fibre lasers based on conventional telecommunication fibres. Furthermore, we present a thorough theoretical description of the phenomenon and demonstrate how our model can be used to predict the observed behaviour, identifying the general requirements for system improvement through RIN transfer reduction.

© 2020 Optical Society of America under the terms of the [OSA Open Access Publishing Agreement](#)

1. Introduction

The concept of laser light generation in cavity-less random active media was introduced by Letokhov in 1966-1968 [1,2], initially in the context of studies of interstellar radiation. Where traditional laser schemes are based on resonant cavities for feedback generation, random lasers use the random multiple scattering of photons in the gain medium, generating a modeless-behaviour laser [3]. Random lasers have attracted a great deal of attention thanks to their unique features, including their relative simplicity and their lack of need for a defined cavity structure [4]. At the same time, their disorderly nature has often become a hindrance to their systematic design and application. A notable exception to this rule is provided by randomly distributed feedback Raman fibre lasers (RDFLs), first proposed in [5] as a particular kind of ultralong fiber laser in which feedback is provided by Rayleigh backscattering spatially distributed along the fibre length. In contrast with other kinds of random lasers, the use of conventional optical fibre as both the gain and transport medium allows for high efficiency, narrow bandwidth and intrinsically directional output [6-9]. Thanks to this, multiple applications in both sensing and communications have become possible [10-12].

Although highly versatile, RDFLs are, like other Raman fibre lasers, limited in their performance by relative intensity noise (RIN) transfer from their pumps. In some of the most useful ultralong RDFL configurations, the need for powerful, also fibre-based and thus intrinsically noisy pumps remains unavoidable. Previous analysis of the RIN transfer in random lasers [13,14] showed the influence of pump power and fibre characteristics on the frequency-dependent RIN transfer function, leading to the presence of multiple regimes, which make determining the optimal configuration for a particular application a daunting task. In previous work [15] we theoretically predicted that in some particular configurations, the maximum RIN transfer in RDFLs that typically happens at low modulation frequencies could be dampened, leading to an anomalous RIN transfer profile in which pump intensity noise is transferred efficiently only to a mid-frequency band, which could help reduce noise impairments in telecommunications and sensing. Recently [16], we presented a particular case for which this effect could be demonstrated experimentally.

In this work we theoretically explore and for the first time experimentally demonstrate this promising regime in a broad range of configurations, which could have great implications in the design of high performance RDFs with reduced noise.

2. Model

The most accurate model to date of RIN transfer from the pump to the Stokes in RDFs was originally proposed in [13], based on the solution of the set of coupled ordinary differential equations (ODEs) describing the average-power evolution of the different components for the pump and Stokes signals (Eqs. (1)–(3)), and then using the obtained solution as an input to the complex set of equations describing the evolution of the amplitude noise spectral density for the same components (Eqs. (4)–(6)):

$$\frac{dP_P^\pm}{dz} = \mp \alpha_P P_P^\pm \mp \frac{\nu_P}{\nu_{S1}} g_1 \left(P_{S1}^+ + P_{S1}^- + 4h\nu_{S1}\Delta\nu_{S1} \left(1 + \frac{1}{e^{h(\nu_P - \nu_{S1})/K_B T} - 1} \right) \right) P_P^\pm \pm \varepsilon_P P_P^\mp \quad (1)$$

$$\begin{aligned} \frac{dP_{S1}^\pm}{dz} = & \mp \alpha_{S1} P_{S1}^\pm \mp \frac{\nu_{S1}}{\nu_{S2}} g_2 \left(P_{S2}^+ + P_{S2}^- + 4h\nu_{S2}\Delta\nu_{S2} \left(1 + \frac{1}{e^{h(\nu_{S1} - \nu_{S2})/K_B T} - 1} \right) \right) P_{S1}^\pm \pm \\ & g_1 \left(P_{S1}^\pm + 2h\nu_{S1}\Delta\nu_{S1} \left(1 + \frac{1}{e^{h(\nu_P - \nu_{S1})/K_B T} - 1} \right) \right) (P_P^+ + P_P^-) \pm \varepsilon_{S1} P_{S1}^\mp \end{aligned} \quad (2)$$

$$\frac{dP_{S2}^\pm}{dz} = \mp \alpha_{S2} P_{S2}^\pm \pm g_2 \left(P_{S2}^\pm + 2h\nu_{S2}\Delta\nu_{S2} \left(1 + \frac{1}{e^{h(\nu_{S1} - \nu_{S2})/K_B T} - 1} \right) \right) (P_{S1}^+ + P_{S1}^-) \pm \varepsilon_{S2} P_{S2}^\mp \quad (3)$$

$$\frac{dn_P^\pm}{dz} + id_P^\pm \omega n_P^\pm = \mp \alpha_P n_P^\pm \mp \frac{\nu_P}{\nu_{S1}} g_1 (n_{S1}^+ + n_{S1}^-) P_P^\pm \mp \frac{\nu_P}{\nu_{S1}} g_1 (P_{S1}^+ + P_{S1}^-) n_P^\pm \pm \varepsilon_P n_P^\mp \quad (4)$$

$$\begin{aligned} \frac{dn_{S1}^\pm}{dz} + id_{S1}^\pm \omega n_{S1}^\pm = & \mp \alpha_{S1} n_{S1}^\pm \mp \frac{\nu_{S1}}{\nu_{S2}} g_2 (n_{S2}^+ + n_{S2}^-) P_{S1}^\pm \mp \frac{\nu_{S1}}{\nu_{S2}} g_2 (P_{S2}^+ + P_{S2}^-) n_{S1}^\pm \pm g_1 (n_P^+ + n_P^-) \\ & P_{S1}^\pm \pm g_1 (P_P^+ + P_P^-) n_{S1}^\pm \pm \varepsilon_{S1} n_{S1}^\mp \end{aligned} \quad (5)$$

$$\frac{dn_{S2}^\pm}{dz} + id_{S2}^\pm \omega n_{S2}^\pm = \mp \alpha_{S2} n_{S2}^\pm \pm g_2 (n_{S1}^+ + n_{S1}^-) P_{S2}^\pm \pm g_2 (P_{S1}^+ + P_{S1}^-) n_{S2}^\pm \pm \varepsilon_{S2} n_{S2}^\mp \quad (6)$$

where ω represents the oscillation frequency, subscripts P, S1 and S2 refer to the pump, first Stokes (signal) and second Stokes (which can be triggered if pump power is high enough) respectively, while signs + and – indicate components propagating in the forward and backward directions. P_i represent the average powers and n_i the amplitude noise spectral densities. Attenuation coefficients are represented by α_i , g is the Raman gain coefficient from the pump to the Stokes and ε_i are the Rayleigh coefficients at each component's optical frequency, ν_i . $\Delta\nu_i$ represent the effective bandwidths for each component. K_B is Boltzmann's constant, h is Planck's constant and T is the absolute temperature of the fiber. Finally, $d_i^\pm = \frac{1}{v_i} \mp \frac{1}{v_{S2}}$ takes into account the different velocities in the transmission and v_i are the group velocities for each component. The system of equations takes into account all relevant effects such as attenuation, pump depletion and Rayleigh backscattering, and is valid to describe any second-order cascaded Raman laser setup, adjusting boundary conditions to define the actual laser architecture (pump location, presence of reflectors, etc.). Please note that the set of equations accounts for the generation and evolution of a second Stokes component, since this plays a relevant role in the observed anomalous RIN transfer response.

Once the solution for $n_s(\omega)$ is found, the RIN transfer function is defined as

$$H_{RIN}(\omega) = \left| \frac{\frac{n_{s1}(\omega)^2}{P_{s1}^2}}{RIN_{in}^2} \right|$$

in order to compare to the electrically measured RIN transfer function, where RIN_{in} is the input optical RIN noise value for the pump. Output laser RIN is mainly proportional to the value of the input pump RIN [17], so in general the RIN transfer function shows little variation for different values of the input pump RIN.

The three most commonly used first-order RDFL configurations [7,18] are summarised in Fig. 1. These include the original centrally-pumped design (a), the more efficient reflector-aided setup (b), as well as the simpler single-pumped lasers (c). Note that case (b) is equivalent to case (a) (for half of the fiber length) in terms of component propagation and behaviour only if the reflector element behaves ideally for both the pump and Stokes components, and similarly case (b) is equivalent to case (c) when reflectivity becomes 0.

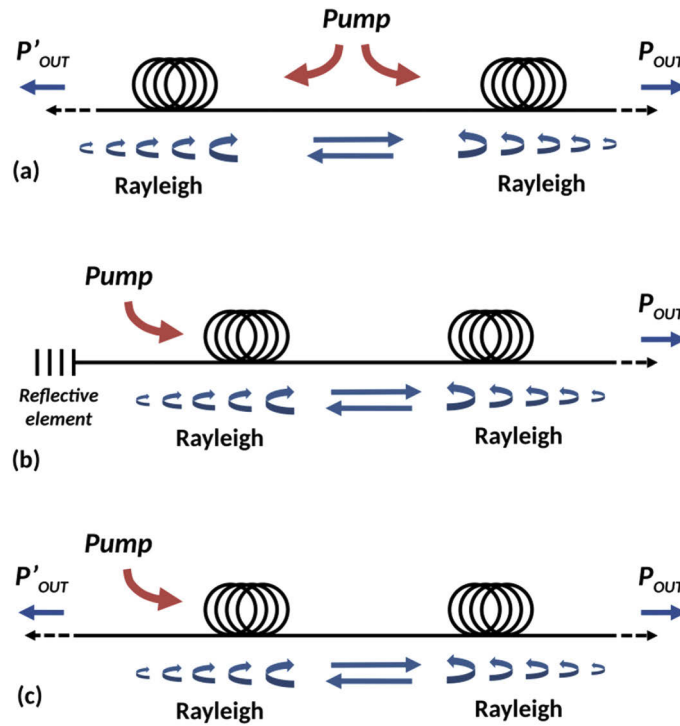


Fig. 1. Schematic depictions of the three RDFL configurations under consideration.

The theoretical performance in terms of RIN transfer has been calculated for the above configurations, using realistic fiber and component characteristics easily replicable in the laboratory. A summary of these results is shown in Fig. 2(a), for the case of 50-km lasers made of standard ITU G652 SMF-28 fiber. Transfer function values in Fig. 2 have been obtained assuming a constant input RIN noise from the pump. Please note that in the centrally-pumped case considered in Fig. 2(a), the pumping point is located at the middle of the 50 km span, with pump power split equally between the two pumps, so the system is equivalent to an “ideal mirror” setup of half the pump power and fiber length.

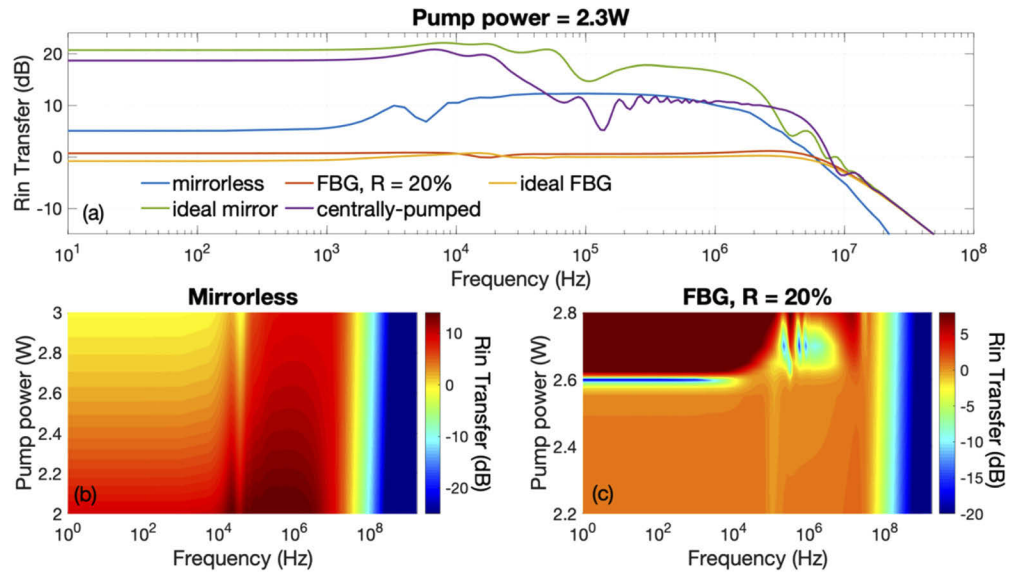


Fig. 2. (a) RIN Transfer for different random laser pumping at 2.3 W for different RDFL configurations. (b) RIN transfer vs. pump power and frequency for the mirrorless case and (c) RIN transfer vs. pump power for the case with a 20% reflectivity reflector at 1550 nm (right)

Interestingly, an anomalous behaviour of the RIN transfer function can be clearly observed for the simplest configuration, the mirrorless scheme corresponding to configuration (c) of Fig. 1, in which a Stokes component at 1550 nm is directly generated by strongly pumping the fibre from one end at 1455 nm. In this configuration, the RIN transfer for the region between 10 kHz and 1 MHz is approximately 7 dB higher than for lower frequencies. On the other hand, when a frequency-selective reflective element operating at the Stokes frequency, such as a fiber Bragg grating (FBG), is located at the pumping fiber-end, this anomalous effect is less evident, even with a low reflectivity (20%), except for a limited range of pump powers, for which the effect can be very intense. For the configuration employing an ideal (100% reflectivity) FBG at 1550 nm, we can observe a slight increase (barely 1 dB) on the RIN transfer between 10 kHz and 20 kHz.

To gather more information about the physical mechanisms at play, which will be explained in more detail in the discussion section, it is convenient to observe the performance dependence with the rise of the pump power, as depicted in Figs. 2(b) and 2(c). For the mirrorless configuration, the RIN transfer is reduced when the pump power is increased. This reduction is higher for low frequencies and it produces a maximum RIN transfer difference between low and high frequencies as the pump power is increased. On the other hand, this effect is less visible for the configurations employing a mirror or FBG, in which the potential RIN transfer reduction is also very high, but restricted to pump powers in the vicinity of the threshold for the second Stokes. This is highlighted in Fig. 2(c), in which the transfer function is almost flat for an extensive bandwidth until the anomalous effect emerges with a reduction of more than 10 dB in the transfer function at low frequencies when the pump power is close to the threshold for lasing at 1645 nm (second Raman Stokes). Above this threshold, RIN transfer is increased, and this effect disappears. This dependence with pump power is similar for any configuration employing a reflector.

When the reflective element is replaced by an ideal mirror capable of reflecting both pump and Stokes signals, or in the equivalent case of a centrally-pumped RDFL configuration, RIN

transfer is always higher for the mid frequencies, and drops quickly after just 20 kHz for every configuration.

3. Experimental results

In order to study the RIN transfer behaviour experimentally, we set up the system schematically depicted in Fig. 3. Here, the setup resembles configuration (b) of Fig. 1, with a recirculating loop mirror acting as the reflector element and a 1555 nm filter with a 0.3 nm bandwidth adding frequency selectivity. Reflectivity was measured at 20%. Two wavelength division multiplexers (WDMs) are used for injecting the pump laser at 1445 nm (IPG Photonics, RLD-5K-1445) into the cavity, which can be made of different Fibers Under Test (FUT) and for removing the residual pump at the output. A fiber isolator at the output is used to avoid reflections.

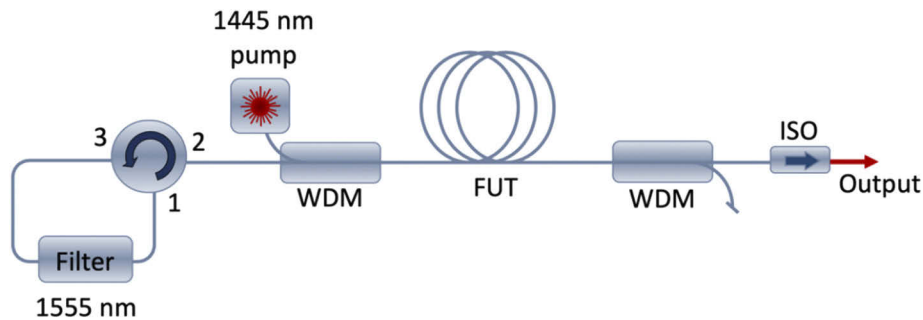


Fig. 3. Schematic of the RDFL setup

The RIN transfer function can be in principle obtained by directly modulating the pump intensity as in [19,20]. However, in our case this approach requires wide bandwidth modulation up to 1 GHz or more. A simpler way to retrieve it is to exploit the intrinsic fiber laser pump RIN, and simply dividing the measured output RIN of the laser by that of the laser pump [21] after careful characterization of both. The available pump operates at 1445 nm, which although does not match the ideal wavelength for maximum Raman gain at the filter's central wavelength of 1555 nm still provides efficient amplification.

The detection method combines two systems, one for the low Fourier frequencies (<10 MHz) and a second one for higher frequencies which could reach up to 6 GHz. For low frequencies, 10 Hz to 1 MHz, a low-noise custom-made photodetector (BW 10 MHz) and a vector signal analyser (FFT Agilent 89410A) were used. On the other hand, for the high-frequency measurements, a fast photodetector with a 6 GHz BW (DS100S) and a spectrum analyser (R&S FSP30) were used. A calibration between both detection systems was carried out showing an offset of about 2 dB, consistent with both the detection system and the analysers' calibration errors. Having more than one decade spectrum overlap between the two detection systems allows for offset removing. An optical spectrum analyser (OSA, Advantest Q8384) with 0.01 nm resolution was used for monitoring the laser spectra.

We carried out the measurement of the RIN transfer function for different fibers; 50 km of SMF G652 and 25 km of TrueWave fiber, and 2.4 km dispersion-compensating fiber (DCF-20). In order to use the same pump power conditions for all the FUT and to operate far from lasing thresholds in all the configurations, we used a pump power of 2.6 W. The output power as well as the physical characteristics of the fibers are summarized in Table 1.

As can be seen in Figs. 4 and 5 below, a reduction in the RIN transfer at low frequencies is evident for both the 25 km TrueWave and the 50 km SMF-based lasers. This reduction apparently increases with fibre length, reaching 5 dB in the 25 km case, but 10 dB in the case of the 50 km

Table 1. System characteristics.

FUT	Output power	Effective Area	D@1.5 μm	α_{1445}	α_{1555}	α_{1650}	ξ_{1555}	ξ_{1650}
SMF 50 km	108 mW	$\sim 70 \mu\text{m}^2$	18 ps/nm km	0.24 dB km ⁻¹	0.19 dB km ⁻¹	0.21 dB km ⁻¹	0.35 W ⁻¹ km ⁻¹	0.27 W ⁻¹ km ⁻¹
TW 25 km	564 mW	$\sim 72 \mu\text{m}^2$	-3 ps/nm km	0.29 dB km ⁻¹	0.20 dB km ⁻¹	0.22 dB km ⁻¹	0.6 W ⁻¹ km ⁻¹	0.36 W ⁻¹ km ⁻¹
DCF 2.4 km	248 mW	$\sim 20 \mu\text{m}^2$	-340 ps/nm km	1.2 dB km ⁻¹	0.6 dB km ⁻¹	0.8 dB km ⁻¹	4.0 W ⁻¹ km ⁻¹	2.5 W ⁻¹ km ⁻¹

fibre. Experimental results exhibit a peak at 600 Hz. This is generated by technical noise coupled to the detection system, and it appears in all the traces presented.

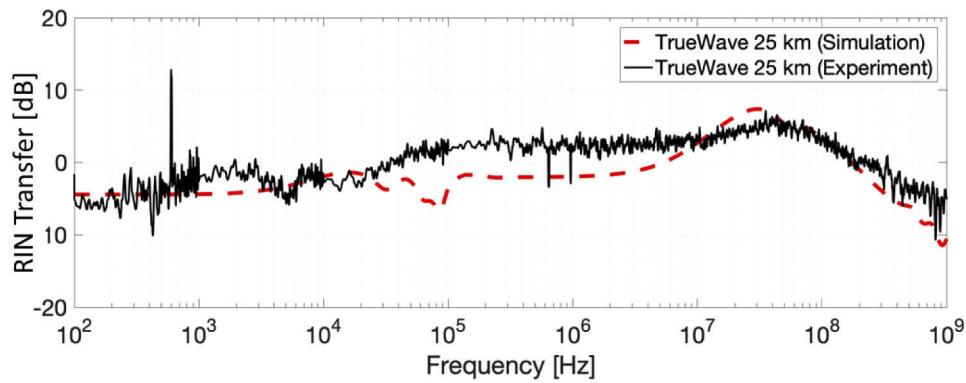


Fig. 4. Measured (black) and simulated (red) RIN transfer curves for the 25 km TrueWave fiber configuration.

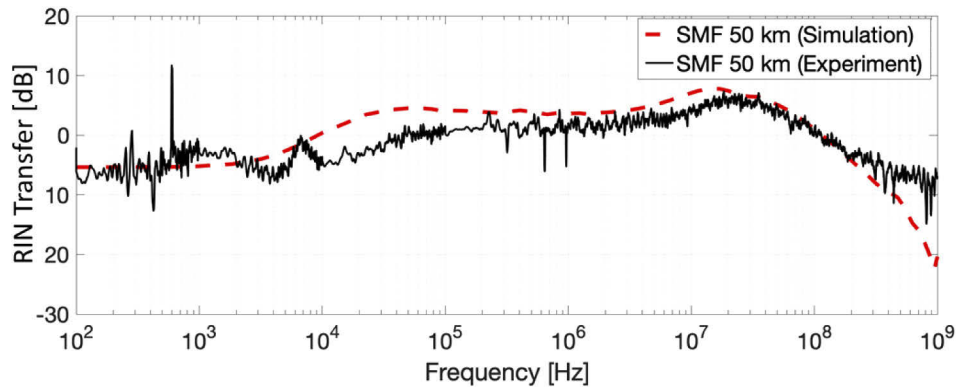


Fig. 5. Measured (black) and simulated (red) RIN transfer curves for the 50 km SMF configuration.

Experimental results are in very good agreement with the simulations, both in terms of the RIN transfer function shape and its magnitude, although limitations in the experimental characterisation of all variables affecting RIN transfer, and in particular the fiber dispersion profile for all the frequencies involved, leads to some noticeable differences between the simulated and experimental curves. Furthermore, there is a certain amount of uncertainty due to experimental

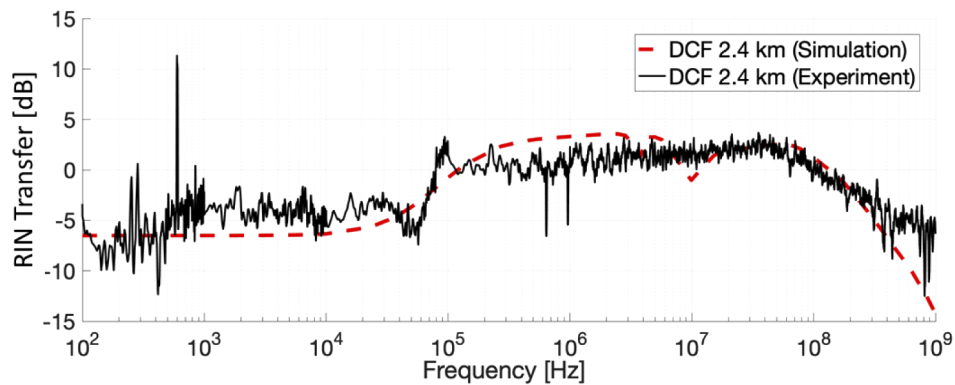


Fig. 6. Measured (black) and simulated (red) RIN transfer curves for the 2.4 km DCF configuration.

limitations in the measurement of RIN at frequencies above 300 MHz. Nevertheless, the anomalous RIN transfer regime is present in all cases.

Similar results are obtained for the significantly shorter dispersion-compensation fiber (Fig. 6), which displays much higher Raman gain and attenuation coefficients. Here the RIN reduction for low frequencies is, once again, close to 10 dB.

4. Discussion

As we have observed, the predicted anomalous reduction of the RIN transfer at low frequencies is easily verifiable at relatively moderate pump powers and using a standard communications fibre. As we will see, the observed behaviour finds its origin in the triple interaction between the generated signal in the counter-propagating direction, the Raman pump and the co-propagating signal. Pump power oscillations at low frequencies suffer more depletion due to oscillations at matching frequencies in the counter-propagating signal. This, consequently, reduces RIN transfer at lower frequencies to the co-propagating generated signal. However, as the RIN transfer to counter-propagating signals has a cut-off frequency close to 10 kHz, this effect is neglected for higher frequencies, becoming non-selective.

This interpretation is compatible with an observed increase of the RIN transfer at low-frequency components in the counter-propagating components, which can be verified by monitoring the RIN at the header of the laser, directly from the output port 3 of the circulator. Figure 7(a) compares the RIN transfer functions at the co-propagating laser output and at the counter-propagating header for the 50 km SMF setup, which as expected display opposite tendencies with regards to low and high-frequency noise.

A more complete picture of the phenomenon can be obtained by artificially turning off specific physical effects in the model, which helps us to understand their relative and combined contribution to the overall RIN transfer function. In the curves in Fig. 7(b), the interactions between pumps and signals in a 50 km length SMF configuration including a frequency-selective 20% reflectivity mirror have been separately turned off, so the individual impact of each contribution can be evaluated. There are mainly two conditions for the observation of the anomalous behaviour:

- The presence of non-negligible Rayleigh backscattering feedback. As it is shown in the figure, if the effect of Rayleigh backscattering is neglected, RIN transfer is constant up to 10 MHz.
- The power of the counter-propagating Stokes signal should be comparable to that of the co-propagating one over the first few kilometres of fibre. This happens always for the

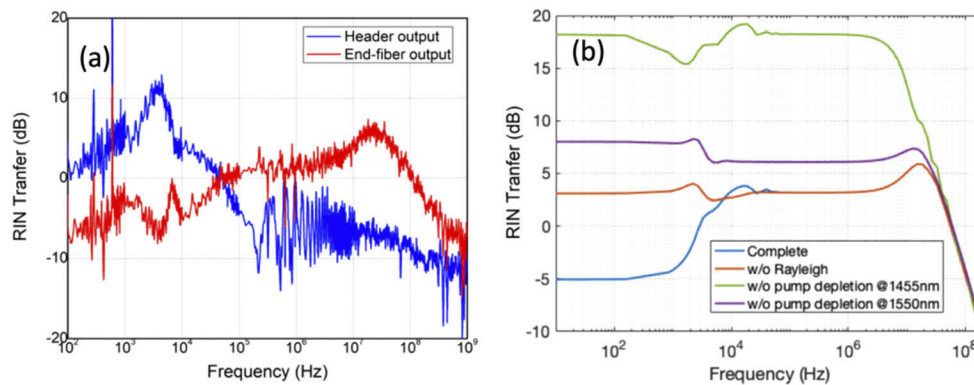


Fig. 7. (a) Comparison between the co-propagating (red) and counter-propagating (blue) RIN transfer functions in the 50 km SMF case. (b) Contribution of different effects to the RIN transfer function in the 50 km SMF configuration.

mirrorless case, as well as for configurations with a reflector when pump power is close to the lasing threshold of the second Stokes. Component depletion, both from the pump and from the Stokes, favors this situation, and indeed if depletion is removed from the model, anomalous RIN transfer cannot be predicted at all.

Perhaps even more interestingly, simulations confirm that these effects contribute to a general reduction of the RIN transfer function. That is, the observed anomalous RIN transfer is not caused by an increase of the RIN at higher frequencies, but to an important reduction of RIN transfer at lower frequencies, which could in turn translate into a noticeable improvement in noise performance for RDFL-based distributed amplifiers for sensing and communications.

5. Conclusion

We have experimentally demonstrated and theoretically described for the first time the reduction of RIN transfer at low frequencies in ultralong random distributed feedback Raman fibre lasers through the interaction between co- and counter-propagating pump and Stokes components. This reduction has been shown to be as important as 10 dB in all the cases considered, which included setups based on 25 km of TrueWave fiber, 50 km of ITU G.652 SMF and a 2.4 km of DCF. Moreover, we have identified the conditions for obtaining a RIN transfer reduction in conventional fibre based random laser setups, showing how this effect can be harnessed through system design, paving the way to its direct application in amplification schemes with application both in sensing and telecommunications.

Funding

Comunidad de Madrid (AEI/FEDER funds TALENTO-CM 2017-T2/TIC-5227, SINFOTON2-CM (S2018-NMT/4326)); Horizon 2020 Framework Programme (Marie Skłodowska-Curie—748839); LAPHIA (Lasers and Photonics in Aquitaine); Conseil Régional d'Aquitaine (2017-1R50302-00013493); Universidad de Alcalá (CCG19/IA-051); Spanish Government (PID2019-107270RB-C22, RTI2018-RTI2018-097957-B-C33).

Acknowledgments

This work has been funded with financial support from the French State, managed by the French National Research Agency (ANR) in the frame of “the Investments for the future” Programme IdEx

Bordeaux – LAPHIA (ANR-10-IDEX-03-02). Conseil Régional d'Aquitaine (2017-1R50302-00013493). Horizon 2020 Framework Programme (H2020) (Marie Skłodowska-Curie—748839). Spanish Government grants RTI2018-097957-B-C33 and PID2019-107270RB-C22. AEI/FEDER funds. Universidad de Alcalá (CCG19/IA-051). Comunidad de Madrid project SINFOTON2-CM (S2018-NMT/4326). JN was supported by Comunidad de Madrid postdoctoral contract TALENTO-CM 2017-T2/TIC-5227.

Disclosures

The authors declare no conflicts of interest.

References

1. V. Letokhov, "Stimulated emission of an ensemble of scattering particles with negative absorption," *JETP Lett.* **5**(8), 212–215 (1967).
2. V. Letokhov, "Generation of light by a scattering medium with negative resonance absorption," *Sov. Phys.-JETP* **26**(4), 835–840 (1968).
3. N. M. Lawandy, R. M. Balachandran, A. S. L. Gomes, and E. Sauvain, "Laser action in strongly scattering media," *Nature* **368**(6470), 436–438 (1994).
4. D. S. Wiersma, "The physics and applications of random lasers," *Nat. Phys.* **4**(5), 359–367 (2008).
5. S. K. Turitsyn, S. A. Babin, A. E. El-Taher, P. Harper, D. V. Churkin, S. I. Kablukov, J. D. Ania-Castañón, V. Karalekas, and E. Podivilov, "Random distributed feedback fibre laser," *Nat. Photonics* **4**(4), 231–235 (2010).
6. S. A. Babin, E. A. Zlobina, S. I. Kablukov, and E. V. Podivilov, "High-order random Raman lasing in a PM fiber with ultimate efficiency and narrow bandwidth," *Sci. Rep.* **6**(1), 22625 (2016).
7. D. V. Churkin, S. A. Babin, A. E. El-Taher, P. Harper, S. I. Kablukov, V. Karalekas, J. D. Ania-Castañón, E. V. Podivilov, and S. K. Turitsyn, "Raman fiber lasers with a random distributed feedback based on Rayleigh scattering," *Phys. Rev. A* **82**(3), 033828 (2010).
8. S. Sigavanam, N. Tarasov, X. Shu, and D. V. Churkin, "Narrow-band generation in random distributed feedback fiber laser," *Opt. Express* **21**(14), 16466–16472 (2013).
9. D. Leandro, S. Rota-Rodrigo, D. Ardanaz, and M. Lopez-Amo, "Narrow-linewidth multi-wavelength random distributed feedback laser," *J. Lightwave Technol.* **33**(17), 3591–3596 (2015).
10. D. V. Churkin, S. Sugavanam, I. D. Vatnik, Z. Wang, E. V. Podivilov, S. A. Babin, Y. Rao, and S. K. Turitsyn, "Recent advances in fundamentals and applications of random fiber lasers," *Adv. Opt. Photonics* **7**(3), 516–569 (2015).
11. M. Bravo, M. Fernandez-Vallejo, and M. Lopez-Amo, "Internal modulation of a random fiber laser," *Opt. Lett.* **38**(9), 1542–1544 (2013).
12. P. Rosa, S. T. Le, G. Rizzelli, M. Tan, and J. D. Ania-Castañón, "Signal power asymmetry optimisation for optical phase conjugation using Raman amplification," *Opt. Express* **23**(25), 31772–31778 (2015).
13. J. Nuño, M. Alcon-Camas, and J. D. Ania-Castañón, "RIN transfer in random distributed feedback fiber lasers," *Opt. Express* **20**(24), 27376–27381 (2012).
14. G. Rizzelli, M. A. Iqbal, F. Gallazzi, P. Rosa, M. Tan, J. D. Ania-Castañón, L. Krzeczanowicz, P. Corredera, I. Phillips, W. Forsysak, and P. Harper, "Impact of input FBG reflectivity and forward pump power on RIN transfer in ultralong Raman laser amplifiers," *Opt. Express* **24**(25), 29170–29175 (2016).
15. J. Nuño and J. D. Ania-Castañón, in *Proc. CLEO EU 2015*, CJ_P_21
16. S. Rota-Rodrigo, D. Leandro, G. Rizzelli, J. D. Ania-Castañón, G. Santarelli, and M. Lopez-Amo, "Experimental observation of anomalous RIN transfer in random distributed feedback Raman fiber lasers," in *Proc. CLEO EU CJ_P_78*.
17. B. Bristiel, S. Jiang, P. Gallion, and E. Pincemin, "New model of noise figure and RIN transfer in fiber Raman amplifiers," *IEEE Photonics Technol. Lett.* **18**(8), 980–982 (2006).
18. W. L. Zhang, Y. J. Rao, J. M. Zhu, Z. X. Yang, Z. N. Wang, and X. H. Jia, "Low threshold 2nd-order random lasing of a fiber laser with a half-opened cavity," *Opt. Express* **20**(13), 14400–14405 (2012).
19. H. Tünnermann, J. Neumann, D. Kracht, and P. Weßels, "Gain dynamics and refractive index changes in fiber amplifiers: a frequency domain approach," *Opt. Express* **20**(12), 13539–13550 (2012).
20. J. Zhao, G. Guiraud, F. Floissat, B. Gouhier, S. Rota-Rodrigo, N. Traynor, and G. Santarelli, "Gain dynamics of clad-pumped Yb-fiber amplifier and intensity noise control," *Opt. Express* **25**(1), 357–366 (2017).
21. S. Rota-Rodrigo, B. Gouhier, M. Laroche, J. Zhao, B. Canuel, A. Bertoldi, P. Bouyer, N. Traynor, B. Cadier, T. Robin, and G. Santarelli, "Watt-level single-frequency tunable neodymium MOPA fiber laser operating at 915–937 nm," *Opt. Lett.* **42**(21), 4557–4560 (2017).